A STUDY OF RR LYRAE STARS

IN THE GLOBULAR CLUSTER IC 4499

A Thesis Presented By
Ana P. Mikler C.

Submitted in partial fulfillment
of the requirements for
Honors in the Department of Physics and Astronomy

UNION COLLEGE
April, 2012

ACKNOWLEDGMENTS

ABSTRACT

MIKLER, ANA P.   A Study of RR Lyrae Stars in the Globular Cluster IC 4499

ADVISOR: Francis P. Wilkin (Union College) and Andrea Kunder (Cerro Tololo Inter-American Observatory)

Observations of the globular cluster IC4499 were taken with the 1m telescope at Cerro Tololo and combined with archival data from multiple telescopes. These data were used to study the variable star population using CCD photometry, with observations in the U, B, V, R and I passbands. The period and the magnitudes have been measured for the RR Lyrae stars. We present light curves in all passbands for all 97 RR Lyrae stars. The magnitudes of the RR Lyrae stars are compared with those measured by Walker and Nemec (1996). The distribution of stars on the horizontal branch is compared with estimates from theoretical models, and we confirm the horizontal branch color limits to the instability strip reported by Walker and Nemec.

I. INTRODUCTION

A. STARS AND THE HERTZPRUNG-RUSSELL DIAGARAM

Current theoretical stellar models have been, for the most part, successful in explaining what we know about ordinary stars. Most of the physical processes that determine the internal structure of a star are very well understood, and stellar evolution has a number of distinct stages that are clearly seen in a Hertzsprung–Russell (HR) diagram. This diagram (see Figure 1.1) shows the relationship between stellar luminosity (or equivalently, absolute magnitude) and spectral type (or effective temperature). In an HR diagram, luminosity increases upwards while temperature increases to the left. In the diagram the stars fusing hydrogen to helium in their core can be identified in the diagonal strip across the plot. The populated regions in the top right show more evolve stars. The evolution of stars will be explained in §C.

In order to relate luminosity and temperature, it is necessary to account for the size of the observed object, in this case the star's radius. Larger stars have a higher cooling rate than smaller stars due to their larger surface area. Using the Stefan-Boltzmann law to relate the star's luminosity to its radius and surface temperature, we obtain

$$L = 4\pi R_*^2 \sigma T^4.$$
<div align="right">1.1</div>

Here, σ is the Stefan-Boltzmann constant, which equals to 5.670 x 10^{-8} J·s^{-1}m^{-2}K^{-4}. Thus, the radius of the star is implicitly known from its location in the HR diagram.
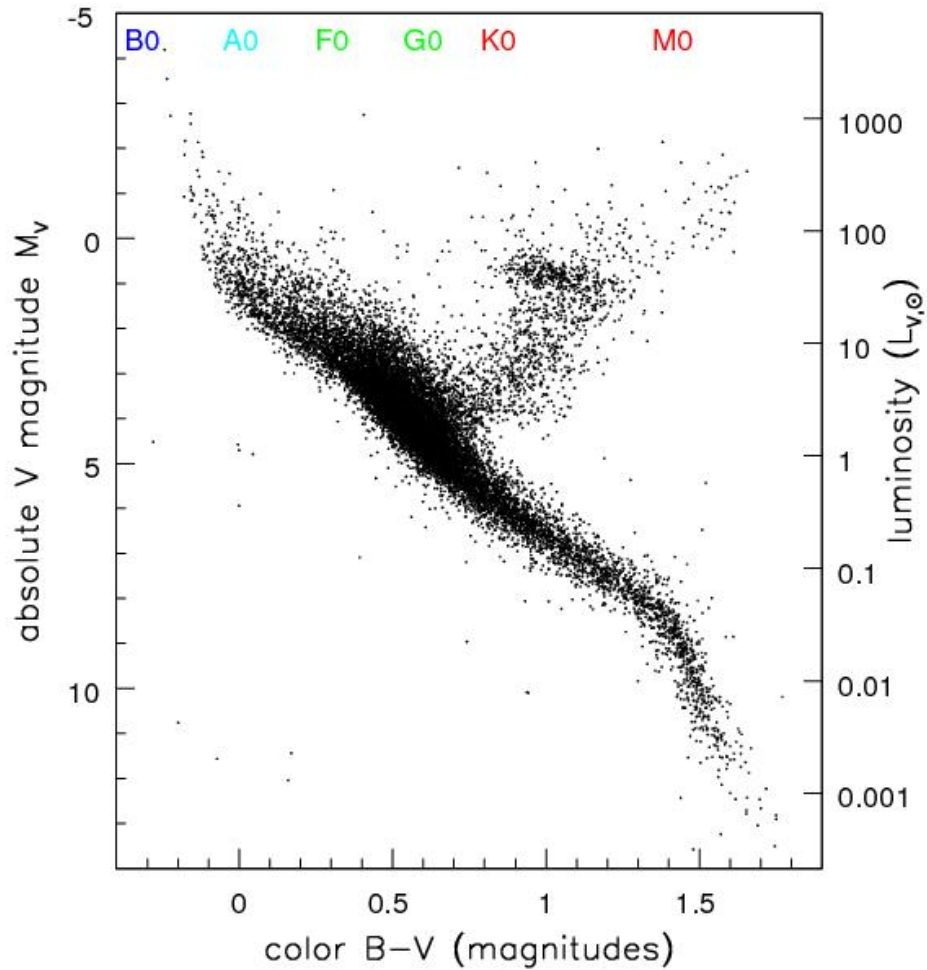
Figure 1.1 An observational Hertzsprung–Russell (HR) diagram for stars within 100 pc of the Sun. Unlike a typical star cluster, the stars shown have variety of ages, metallicities as well as masses. Spectral type is shown on the top x-axis.[1]

B. BASIC PHYSICS OF STELLAR STRUCTURE

The mass, luminosity and surface temperature of a star can be modeled using the equations of stellar structure. These equations assume that stars are spherically symmetric and in a steady state. They represent the dependence of mass, pressure, temperature and luminosity with interior radius. To describe such a relationship we assume a spherical shell of thickness dr at a distance r from the center of the star.

---

[1] Perryman, M.A.C *et al*. 1195, A&A, 304, 69.

Stars are observed to be in hydrostatic equilibrium, where the inward force created by gravity balances the outward force produced by the pressure gradient. Equation 1.2, describes this relationship

$$\frac{dP}{dr} = -G\,\frac{M_r \rho}{r^2} \qquad (1.2)$$

where G is the gravitational constant, M_r is the mass inside the radius r, ρ is the density and P is the pressure. According to Gauss' law, by spherical symmetry, the gravitational field at any location depends only upon the interior mass, and upon the radius. This interior mass of the star is given by

$$\frac{dM_r}{dr} = 4\pi r^2 \rho \qquad (1.3)$$

Then, by integrating this equation from zero to the star's radius, we can obtain the total mass of the star.

Furthermore, the luminosity exiting a given radius is given by the integrated energy generation rate in the interior:

$$\frac{dL_r}{dr} = 4\pi r^2 \rho \epsilon \qquad (1.4)$$

where ϵ is the energy generation rate per unit mass, which is non-zero only in the region where nuclear reactions occur.

Finally, the energy transport in a star can be expressed in different forms depending on the type of transportation.

$$\frac{dT}{dr} = -\frac{3}{4ac} \frac{\bar{\kappa}\rho}{T^3} \frac{L_r}{4\pi r^2}, \quad \text{(Radiative)} \tag{1.5}$$

$$\frac{dT}{dr} = -\left(1-\tfrac{1}{\gamma}\right) \frac{\mu m_H}{k} \frac{GM_r}{r^2}, \quad \text{(Convective)} \tag{1.6}$$

The previous equations are time independent for very slow evolutionary stages. To integrate them, we must also know the constitutive relations which describe the pressure P, energy generation rate ε, and opacity κ as a function of temperature, density, and chemical abundance. These relationships implicitly include such effects as changes in the ionization fraction and excited electron states of atoms and ions.

C. STELLAR EVOLUTION

Due to chemical composition changes and their loss of energy stars must evolve. This creates changes in the star's surface temperature, luminosity and radius that can be seen in an HR diagram. A theoretical HR diagram is shown in figure 1.2, the Main Sequence (MS) region represents most of the lifetime of a star. During this stage, stars fuse hydrogen to helium in their core, until the core runs out of hydrogen. Then, they continue fusing hydrogen to helium in a shell just outside the core, increasing their luminosity somewhat and slightly cooling as sub-giants. At this point stars are no longer on the MS, and they move along the sub-giant branch to the right in the HR diagram, until the core becomes degenerate. From then on the star's atmospheric temperature is approximately constant and its luminosity increases as it moves up the red giant (RG) branch. At this point, the star continues fusing hydrogen to helium in a shell outside the core as during the SG evolution, but now the core is degenerate. Due to the lower

temperature of the star, it is seen as orange or red, so stars at this stage are called red giants (RGs).

Stars remain RGs until their core is hot enough to start fusing helium to produce carbon. This is called the helium flash when ignition occurs in a degenerate core, appropriate for low-mass stars. Once stars fuse helium in its core, the core re-expands such that its luminosity decreases until it reaches equilibrium between energy generation rate in core and luminosity. Their luminosity remains approximately constant, while the surface temperature increases. This stage is called the Horizontal Branch (HB), shown as part E in Figure 1.2.
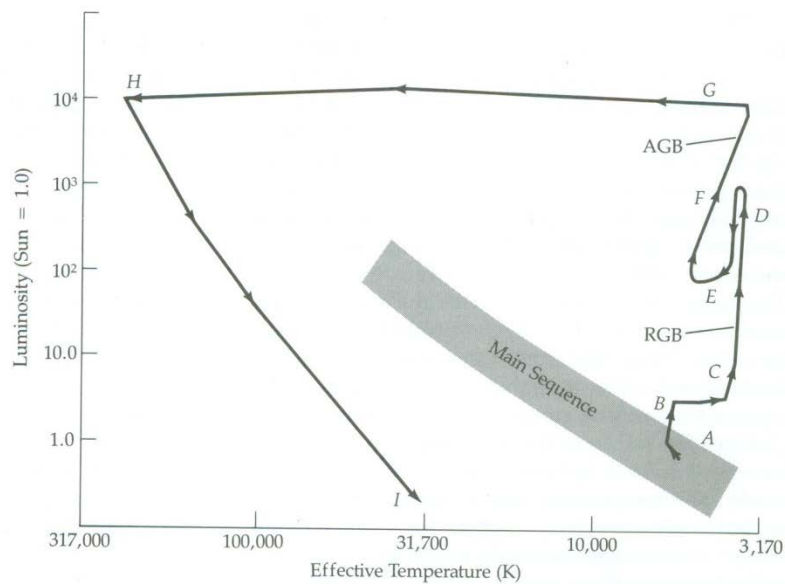

Figure 1.2 A theoretical Hertzsprung–Russell (HR) diagram. Stars with different masses stay on the main sequence for most of their lifetime. Then they evolve from the main sequence. The evolutionary track of a sunlike star is shown[2].

---

[2] Michael Zeilik and Elske v. Smith. *Introductory Astronomy & Astrophysics* (Philadelphia:Saunders College Publishing 1987) p. 284

Within the HB there are some stars whose thermal pressure gradient and gravitational force are not able to achieve stable equilibrium and therefore these stars pulsate. Additionally, their luminosity fluctuates periodically, so that the stellar (atmospheric) luminosity matches the core luminosity on average only. This occurs because of changes in the degree of ionization in the outer layers of the star. When the star expands, the atmospheric temperature decreases and with it the degree of ionization, making the star more transparent. Similarly, when the star contracts the degree of ionization increases making the star more opaque, consequently the gas heats up again and the star starts expanding again. This phenomenon is referred to as the κ-mechanism after the symbol used for the opacity. These pulsating stars are found on the HR diagram in a region called the instability strip (IS). This thesis focuses on the pulsating stars found on the HB, known as RR Lyraes after their prototype RR Lyraes.

D. STELLAR PULSATION AND RR LYRAE STARS

The RR Lyrae stars inhabit the horizontal branch of the HR diagram and pulsate radially with periods in the range of 0.2 to 1.0 days. They are mostly present in globular clusters (GC) and the dwarf galaxies in the neighborhood of the Milky Way (Cortes and Catelan 2008). Due to their wide range of metal abundances, and their great ages (Walker *et al*. 2011), GCs are key ingredients in any explanation of the stellar and chemical evolution of our galaxy. RR Lyraes once had a similar mass to our sun, are old and metal-poor. They are more common than most other pulsating stars, with the notable exception of delta Scuti stars, but they are also less luminous than Cepheid variables or "long-period variables".

There is an approximate relationship between pulsation period Π and average density ρ given by

$$\Pi = \sqrt{\frac{3\pi}{2\gamma G\rho}} \qquad\qquad (1.7)$$

Due to the well-known relationship between their pulsation period and their absolute magnitude, they are used as 'standard candles' for distance determinations of objects within the Milky Way and also for distance indicators to nearby galaxies. (The use of standard candles will be explained in §H.) RR Lyraes are divided into 4 different categories based on the period of the stars: RRab, RRc, RRd and RRe. The most common RR Lyraes are of type RRab.

E. THE INSTABILITY STRIP

RR Lyrae stars are found in the instability strip on the HR diagram (Figure 1.3). In order to determine the color limits of the strip different methods have been developed. Walker and Nemec (1996) used the Lee HB parameters to determine the color boundaries. These parameters are determined by characterizing the distribution of the horizontal branch stars based on the metallicity, age and RGB mass loss. Then, considering these parameters and the distribution of the RR Lyraes across the different categories of RR Lyraes, the instability strip limits were determined using evolutionary model tracks. Walker and Nemec compared their observations with the evolutionary model tracks.
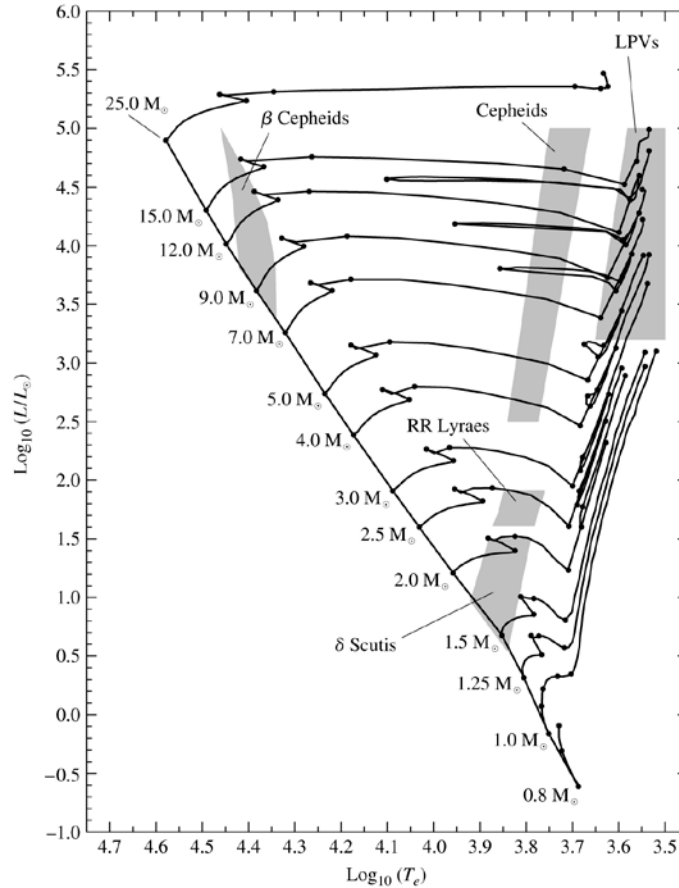
Figure 1.3. HR diagram for multiple stellar masses, where the evolutionary track is   shown. The shaded regions represent the instability strip regions for the multiple variable stars[3].

F. MAGNITUDES AND COLOR INDEX

The magnitude of a star refers to its brightness, the higher the brightness of a star the lower the number of its magnitude. There are apparent and absolute magnitudes. An apparent magnitude (m) is the measurement of the brightness of a star seen from Earth corrected for the effects of the atmosphere. The apparent magnitude is related to the received flux (after correction for the atmosphere) by Pogson's equation

---

[3] Bradley W. Carrol and Dale A. Ostile, *An introduction to Modern astrophysics* (San Francisco:Pearson Addisson Wesley 2007) p.227

$$m = k - 2.5 \, log_{10}F, \hspace{4cm} 1.8$$

where k is a constant that determines the zero-point of the magnitude scale and depends on the filter band. Equation 1.8 shows a logarithmic relation between magnitude and flux; this is because apparent magnitudes were measured with the eyes, and since the eye's sensitivity is logarithmic, the magnitude scale is too. The absolute magnitude (M) denotes the intrinsic brightness and is defined as the apparent magnitude a star would have if it were a distance of 10 parsecs from Earth. It is related to the star's apparent magnitude and distance by

$$m = M + 5 \, log_{10}(d/10 \text{ pc}) \hspace{4cm} 1.9$$

In order to measure the brightness at different wavelengths, images of the stars are taken using different standard filters, usually denoted UVBRI. These passbands go from the near ultraviolet to the near infrared. Table 1.1 shows the peak wavelength and width for the UVBRI passbands.

FILTER	PEAK WAVELENGTH (nm)	WIDTH[a] (nm)
U	350	70
B	435	100
V	555	80
R	680	130
I	800	150

Table1.1 Wavelength ranges of various filters, where the width is the full width half maximum.

Using the apparent magnitudes of the stars in each filter, we can obtained a quantitative measure of the color by calculating the apparent magnitude difference between two passbands

(technically called the color index). Colors are indicators of temperatures due to the near-blackbody nature of stars. For RR Lyraes, color changes cyclically during the pulsation. RR Lyraes usually lie between (B-V) = +0.20 and (B-V)=+0.50, redder than the standard star Vega which is defined to have color (B-V) = 0.0.

The color and magnitude of a star can be related through a color-magnitude diagram (CMD). This diagram is a type of HR diagram where the vertical axis is the apparent or absolute magnitude of the stars and the horizontal axis is the index color. Commonly the x-axis is in the B-V, B-I or V-I color, and the y-axis is in the V magnitude. For such diagrams it is necessary to know the distance and the interstellar reddening of the stars. If the apparent magnitude of the stars is used, it is necessary to plot stars that are observed at the same distance. Then CMDs are highly used for star clusters.

G. CCD PHOTOMETRY

Photometry is the method by which we determine the brightness of a star. In astronomy CCD Photometry is typically used. CCD stands for charge-coupled device, the standard camera detector which is a semiconductor capacitor that converts voltage into a digital signal. The basic mechanism is the photoelectric effect, whereby an incident photon dislodges an electron in the semiconductor. The CCD camera is opened to collect photons for a definite period of time, termed the exposure time. After the exposure time is over, electrons are read out on a pixel-by-pixel basis. In fact, the ratio of detected incident photons to photoelectrons is not unity, but is given by the camera gain factor.

However, it is necessary to account for background noise and other corrections that are introduced with the use of the CCD. For every image taken with a CCD camera it is necessary to apply bias, dark and flat-field corrections. For this thesis, the images used were obtained from archival data and such reductions were performed previously to our use. The following explains the purpose and general procedure of the different reduction. However, because we did not perform the reductions only the theory is explained below but not the specifics of the calibration process for the images. Bias counts are added to every image taken by the CCD camera to avoid negative values in the read out, which may occur due to read out noise. In order to remove these extra counts, images with zero exposure time are taken, and subtracted from the raw image. This procedure is called a bias subtraction. It is also possible to obtain some "false" counts in the images taken, due to dark current. This represents electrons that did not result from the photoelectric effect, but were instead excited thermally. Dark correction refers to subtraction from the image of a dark frame suitably weighted by exposure time. Finally, a flat correction is necessary in order to obtain uniform illumination in the image taken. The images taken have to be divided by flats, which are pictures of a white screen or twilight/dawn sky. These flats have to be taken on the same night as the observations are taken and with each filter used.

After all the corrections are applied to the images, photometry is performed to determine the magnitudes of the stars observed. The method used to perform photometry involves a point spread function (PSF) fitted to every star observed. The PSF describes the combination of diffraction pattern at the CCD of a point source and the atmospheric seeing (it is

normally dominated by seeing for ground-based observations). This PSF photometry is especially important in crowded star fields such as those of globular clusters.

H. DISTANCE DETERMINATION

To determine the distance to distant celestial objects it is necessary to use the method of standard candles, which uses an object for which the luminosity (or equivalently, its absolute magnitude M) is known. There exist multiple standard candles such as type 1a supernovae, planetary nebulae and variable stars. Cepheid variables and RR Lyrae stars are variable stars that are also used as standard candles. The luminosity of RR Lyrae stars can be obtained from their relationship between the period and luminosity as shown in Catelan et al. (2004). Although the best relationship between period and luminosity is determined in the K passband, at wavelength 2.2μm, we used the I band to determine the luminosity, which is given by

$$M_I = 0.471 - 1.132 \log P + 0.205 \log Z, \qquad\qquad 1.10$$

where P is the pulsation period of the star and Z is the metallicity. Once the absolute magnitude for the RR Lyrae star is obtained, we can determine its distance using equation 1.9.

I. IC4499

The study of GCs allows us to understand better the early evolution of the Milky Way and its system of GCs. However, many of the GCs found show the presence of multiple populations (Walker et al. 2011) making their study harder. IC 4499 shows a single population that contains sufficient stars for population analysis. The properties of this cluster should be consistent with the properties of other GCs.

IC 4499 was discovered in 1901 by D. Stewart and is only visible in the southern hemisphere at R.A 14h 52m 10s, DEC -82° 00'48". It is a low density globular cluster, notable for its large number of RR Lyrae variable stars and young age.

II. OBSERVATIONS AND DATA REDUCTION

A. OBSERVATIONS

CCD images of IC4499 were obtained from archival data spanning over 10 years. The observations were made with the 0.9m, 1.0m, 1.5m and the 4.0m "Blanco" telescopes at Cerro Tololo, as well as the New Technology Telescope (NTT) at La Silla and the 6.5m Magellan telescope at Las Campanas Observatory. There are 200-300 standard stars in each image, depending on the filter.

The reductions were done using either dome flats from a white screen, or twilight flats. After these corrections were applied, point spread function photometry and periods were obtained for the variable stars. These data come from Peter Stetson of the University of Victoria, who reduced and performed crowded field photometry.

B. COLOR- MAGNITUDE DIAGRAMS

To study the RR Lyrae stars in IC4499, we first created a color-magnitude diagram, plotting V vs. (B-V). We determined the age of the cluster by overlaying isochrones (which mean equal-age) curves in the CMD and choosing the best fit visually. The isochrones came from the BaStI (http://albione.oa-teramo.inaf.it/) database, and we fixed the distance modulus and reddening[4] to known values, while adjusting the metalicity and age. Figure 2.1 shows the CMD for IC4499 with the best-fit isochrones corresponding to an age of 13 Gyr.

---

[4] Reddening refers to the extinction occurred due to the light scattering by dust. This causes changes in the spectrum of electromagnetic radiation produced by a source. It is sometimes referred to as the color excess, which refers to the difference between the object's observed and intrinsic color index.
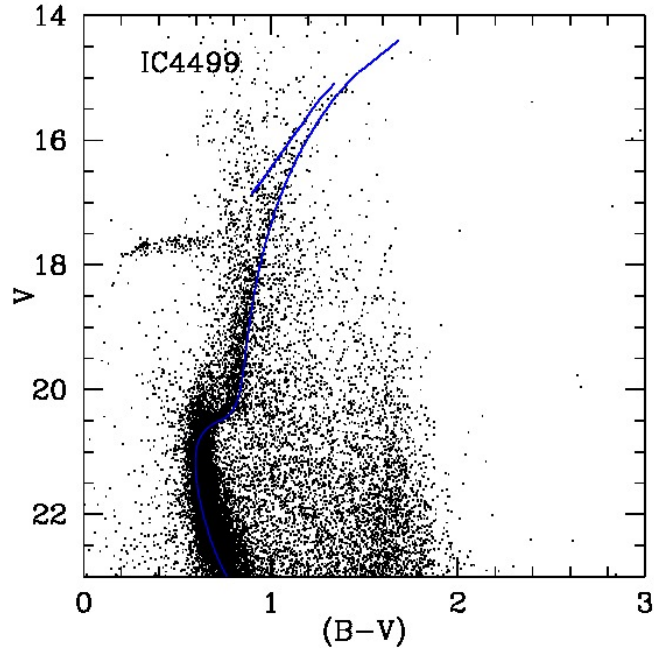
Figure 2.1. Color--magnitude diagram for IC4499 after field star subtraction. The blue curve indicates the best matching isochrone from the BaSTi models corresponding to 13 Gyr.

C. FIELD STARS

Once we obtained an isochrone with a good match to the observational data, we removed the field stars so as to be able to determine which stars belong to the HB. In order to do this, we used a similar method to the one described in Gratton et al. (2010), where they identify the field stars using the Trilegal code, which is a population synthesis model for simulating the stellar photometry of any field in the Galaxy.

Instead of using the Trilegal code, however, we opted for the Besancon model (Robin et al. 2003) of the Galaxy. This is because with Trilegal, one needs to know the star formation history of the galaxy field being studied. The Besancon model produces a synthetic stellar population of the Milky Way and hence gives a global view of the Galaxy including dynamical and

evolutionary aspects. The resulting model can be used for simulations of the galactic stellar populations in any direction. Hence, this code allows one to know, on a statistical basis, how many field stars are in the area of the cluster and their resulting magnitudes and colors.

Running the Besancon model with the specific input parameters, we wrote a program that reads the output from the model and matches the closest field star predicted to an observed star in our CMD. Our program then removes these predicted field stars provided they do not differ too much from the predicted properties. Specifically, the program takes the difference in the (B-I) colors of all data points (i.e., the (B-I) from the model and the (B-I) from the observations) and selects stars that are within a Δ(B-I) of 0.3 mags. Then, the star in the field of view corresponding most nearly in (B-I) to a predicted field star (the star with the smallest difference in (B-I) color) is flagged. Finally, the stars that did not correspond closely to a field star were saved and plotted on the CMD.

D. MAGNITUDES

After the field stars were removed from our IC4499 sample, we selected only the stars on the horizontal branch. We, then, divided those stars into three groups: RR Lyraes, and those to either side of the instability strip, which, here, we refer to as "red" and "blue" stars. We determined the number of stars in each of these three groups. The boundary conditions in color (B-V) for the red and blue edges of the instability strip were obtained from Walker & Nemec (1996).

Pulsation periods were obtained for all the RR Lyrae stars by Peter Stetson. We used these periods and our magnitudes to determine the intensity mean magnitudes, magnitude mean

colors and light curve amplitudes. The intensity mean magnitude uses Pogson's equation and the mean flux over the cycle. (Intensity mean magnitude is a term used in the literature, but since the stars are unresolved, it should really be called flux mean magnitude). The magnitude mean color is defined as the difference between two intensity mean magnitudes, corresponding to two different filters. We fitted standard light curve templates to the observed RR Lyrae light curves using the stdlc Fortran program from Layden (1998). This program requires the period of each star (which has been previously determined) and the observed magnitudes in each filter as a function of time. The program fits ten templates to the data and gives statistics of the best 4 fits. Finally we visually choose the best fit of those four. Once the best fit was chosen, a plot of the light curve was created. The program yields the intensity mean magnitude for the fitted template and from the observed data.

After running Layden's program, we obtained 5 different light curves for each star, one for each filter, that were then combined into a single plot. Figure 2.2 shows an example of the light curves in multiple filters combined in one plot for one star. The values for intensity mean magnitude, mean color and amplitudes given by the code for the observed data were compiled in tables, for each type of RR Lyrae star. Most of the data fitted the theoretical templates well.

However, due to the heterogeneous instrumentation used to obtain the data, in some cases it was necessary to divide the observed data into two sets and have different templates fitting them. Then, in order to obtain the mean magnitude, mean color and amplitude of those light curves, we averaged the values obtained for each set of data. Furthermore, the observations in the U filter for some of the stars were not sufficient to obtain a good match with the theoretical templates. In those cases, values for the U filter were not used.
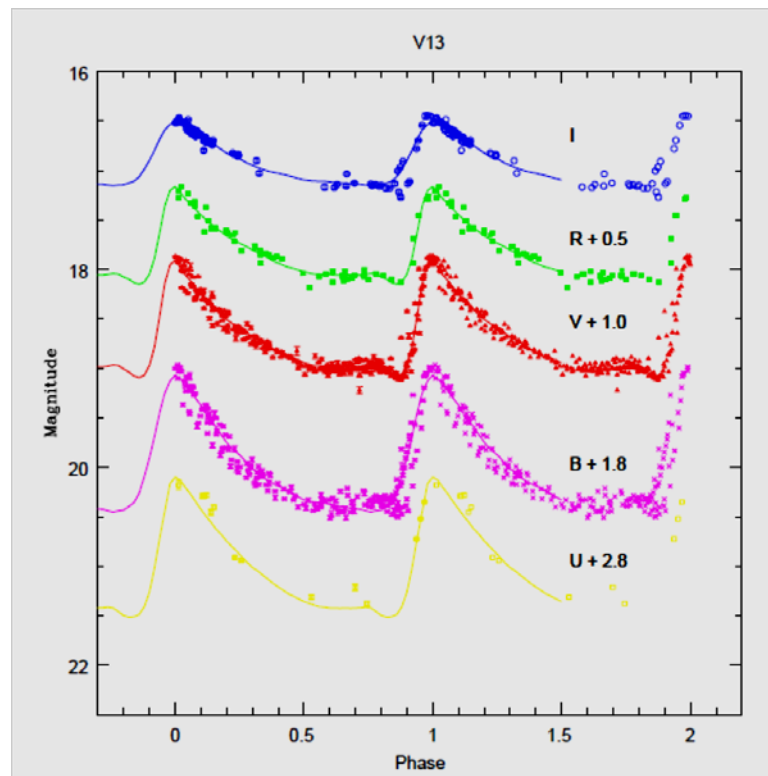
Figure 2.2. Light curves in multiple filters for one of the RR Lyrae stars in the GC IC4499.The solid lines represent the templates from the model and the dots are the observed data.

E. THE INSTABILITY STRIP

In order to determine the color boundaries of the instability strip for IC4499, we used a code that predicts how many blue, red and RR Lyrae stars should be present in a GC with similar

characteristics to those of IC4499. We assigned the mass, age, metallicity and total number of HB members within IC4499. In order to obtain statistically correct values we used a larger stellar population than the one observed in IC4499. Then, we corrected for this by dividing the number of stars by the appropriate factor.

Once we had a good sample of the HB stars from the model, we over-plotted the stars given by the model with the data (mean magnitudes and mean color) obtained from the light curves. We then limited our theoretical RR Lyraes to the same color limits reported by Walker & Nemec (1996) and superimposed the data from the light curves. We checked to determine if the instability strip given by Walker et al. (2011) enclosed all of our RR Lyraes. Thus, we were able to confirm the limits of the instability strip in (B-V) color. With the instability strip determined, we compared the number of stars we observed in each group with the values given by Walker & Nemec (1996). We also compared our intensity mean magnitudes, mean colors (from intensity mean magnitudes) and light curve amplitude values with those from Walker & Nemec.

III. RESULTS AND DISCUSSION

A. COLOR-MAGNITUDE DIAGRAM AND THE AGE OF IC4499

After applying field star subtraction, a color-magnitude diagram was created and overplotted with an isochrone. Figure 2.1 shows the CMD in V versus (B-V) along with this isochrone. We limited the data sample to sources projected within the tidal radius of the cluster, which was determined to be 12.35 arc minutes. We obtained several parameters from the literature, including the distance modulus, DM_o = 16.47, and color excess, E(B-V) = 0.23 from Cardelli et al. (1989) and the cluster metallicity [Fe/H] = -1.52 ± 0.12 from Hankey & Cole (2010). The chosen isochrone matched as closely as possible the above values. This isochrone also used canonical parameters compared to similar GCs: α-enhanced abundance, [α/Fe] = +0.4, low metalicity Z=0.0006, ratio of total to selective extinction R_v = 3.1 and DM_o = 16.4, with the last value similar to that given by Walker et al. (2011). We determined the best fit visually, by matching as closely as possible the main sequence turnoff of the CMD. We found the age of the GC to be $12.5^{+0.5}_{-1.5}$ Gyr, which agrees within the uncertainty with that reported recently by Walker et al. (2011), and disagrees with earlier studies suggesting IC 4499 was a younger than average GC (Ferraro 1995). This age indicates that IC4499 is older than most other GCs in the galaxy, although its metallicity is near the peak of the metallicity distribution for GCs in our galaxy (Zinn 1985).

B. MAGNITUDES AND PERIOD-LUMINOSITY RELATIONSHIP

Once we determined an age for the cluster, we obtained fits to the RR Lyrae photometry for intensity mean magnitudes and light curve amplitudes. These values are reported in Table

3.1. Furthermore, we found 3 independent magnitude mean colors (Table 3.2). Comparing our results to Walker and Nemec (1996), we have obtained more precise periods, as indicated by our smaller uncertainties. We also confirm that the stars reported previously in each RR Lyrae category are consistent with our results, with the exception of V81 whose new period agrees with those for type RRe. V81 was classified as RRc by Walker & Nemec, although both that study and the current work had difficulties in obtaining a good fit. Further study is needed. Furthermore, within the category RRab, some stars are found to have a smaller period than previously reported. However, the number of stars of type RRab is consistent with previous results.

RRe											
V	Period (d)	<B>	<V>	<R>	<I>	<U>	A_B	A_V	A_R	A_I	A_U
1575	0.279667	18.035	17.661	17.37	17.084	18.181	0.518	0.328	0.269	0.251	0.373
81	0.2844449	17.874	17.374	17.011	16.637	17.991	0.618	0.443	0.366	0.176	0.439
153	0.2858137	18.089	17.708	17.454	17.077	18.256	0.51	0.382	0.342	0.304	0.303
97	0.28825486	18.021	17.64	17.373	17.05	18.152	0.633	0.467	0.356	0.287	0.473
56	0.28954261	18.103	17.704	17.407	17.08	18.185	0.795	0.66	0.493	0.374	0.74

RRd											
V	Period (d)	<B>	<V>	<R>	<I>	<U>	A_B	A_V	A_R	A_I	A_U
78	0.3457417	18.272	17.774	17.447	17.051	18.472	0.879	0.699	0.570	0.427	0.388
18	0.3522698	18.167	17.739	17.363	16.993	18.335	0.929	0.923	0.582	0.444	0.282
65	0.3527580	18.105	17.655	17.314	16.941	18.245	0.819	0.689	0.551	0.420	0.338
10	0.3532003	18.140	17.665	17.366	16.943	18.166	1.008	1.001	0.578	0.471	1.040
21	0.3533424	18.159	17.708	17.422	16.963	18.257	0.844	0.673	0.506	0.353	0.601
51	0.3551330	18.122	17.654	17.313	16.960	18.158	0.742	0.846	0.377	0.285	0.469
109	0.3555176	18.210	17.740	17.391	17.000	18.401	0.715	0.569	0.483	0.227	0.584
59	0.3572801	18.157	17.668	17.347	16.968	18.178	0.795	0.581	0.424	0.368	0.496
87	0.3577057	18.152		17.351	16.952	18.299	0.907		0.532	0.412	0.606
63	0.3577295	18.203	17.728	17.386	16.979	18.293	0.802	0.661	0.552	0.371	0.487
93	0.3591978	18.155	17.671	17.331	16.940	18.231	0.954	0.760	0.646	0.418	0.543
73	0.3661399	18.095	17.681		16.976	18.187	0.782	0.720		0.448	0.494
42	0.3725726	18.069	17.625	17.265	16.916	18.103	0.775	0.624	0.321	0.381	0.566
31	0.3617416	18.136	17.668	17.374	16.929	18.320	0.982	0.789	0.623	0.530	0.344
90	0.3635950	18.075	17.600	17.299	16.895	18.142	0.794	0.665	0.475	0.382	0.600
8	0.3673849	18.124	17.664	17.249	16.940	18.250	0.923	0.777	0.549	0.408	0.548
71	0.3693186	18.112	17.634	17.292	16.956	18.264	0.880	0.780	0.712	0.334	0.392

Table 3.1. Derived parameter values for the RR Lyraes, where V indicates the star number; <B>, <V>,<R>, <I> are the intensity mean magnitudes; and A_B, A_V, A_R, A_I are the light curve amplitudes in each filter. Stars are divided by categories, which are determined by period. The tables are ordered by the star's period.

					RRc					
V	Period (d)	<B>	<V>	<R>	<I>	<U>	A_B	A_V	A_R	A_I	A_U
103	0.35298342	18.139	17.69	17.346	16.99	18.229	0.71	0.586	0.407	0.339	0.465
77	0.35464192	18.106	17.664	17.331	16.971	18.086	0.668	0.499	0.388	0.299	0.356
92	0.3547447	18.185	17.721	17.393	17.002	18.305	0.607	0.501	0.305	0.279	0.375
89	0.35538932	18.139	17.682	17.347	16.976	18.251	0.868	0.551	0.469	0.311	0.556
98	0.35564213	18.189	17.719	17.455	17.016	18.24	0.596	0.468	0.254	0.278	0.343
111	0.35734358	18.124	17.67	17.384	16.964	18.208	0.59	0.85	0.346	0.282	0.491
96	0.3584335	18.12	17.653	17.321	16.946	18.193	0.668	0.617	0.395	0.312	0.507
55	0.3585305	18.115	17.664	17.321	16.961	18.222	0.718	0.594	0.418	0.284	0.406
434	0.359564	14.807	14.367	14.047	13.648	14.985	1.076	0.557	0.422	0.343	0.533
32	0.3599885	17.859	17.293	16.877	16.439	17.972	0.514	0.399	0.246	0.254	0.371
95	0.36264582	18.156	17.688	17.332	16.961	18.229	0.677	0.582	0.381	0.306	0.454
29	0.36268588	18.105	17.646	17.313	16.956	18.17	0.733	0.534	0.386	0.341	0.979

					RRab					
V	Period (d)	<B>	<V>	<R>	<I>	<U>	A_B	A_V	A_R	A_I	A_U
3	0.4832464	18.16	17.717	17.351	17.002	18.246	1.595	1.269	0.942	0.802	1.335
40	0.485722	18.47	17.907	17.096	17.116	18.542	1.507	1.232	0.795	0.737	0.473
34	0.4935571	18.109	17.688	17.495	16.965	17.903	1.576	1.255	0.661	0.856	1.501
2	0.4936367	18.129	17.675	17.296	16.949	17.993	1.556	1.273	0.993	0.839	1.457
17	0.4980768	18.168	17.685	17.329	16.944	18.033	1.645	1.375	0.947	0.998	1.576
49	0.499113	18.247	17.698	17.364	16.98	18.446	1.007	0.587	0.511	0.296	0.397
14	0.5003413	18.065	17.651	17.287	16.953	18.278	1.727	1.426	0.938	0.746	1.001
58	0.5005887	18.196	17.698	17.34	16.955	18.251	1.254	0.876	0.515	0.526	0.825
33	0.5063625	18.691	17.933		17.162	18.72	0.249	0.658		0.277	0.157
27	0.5067589	18.216	17.697	17.361	16.952	18.269	1.47	1.201	0.899	0.761	1.33
23	0.5077039	18.131	17.702	17.327	16.988	17.944	1.626	1.302	1.032	0.707	1.599
13	0.5115214	18.116	17.65	17.283	16.925	18.044	1.544	1.355	1.021	0.824	1.201

24	0.5165604	18.164	17.665	17.279	16.888	18.132	1.398	1.1	0.797	0.585	1.413
57	0.5169378	18.229	17.739	17.364	16.966	18.234	1.531	1.239	0.733	0.579	1.077
48	0.5197904	18.128	17.651	17.345	16.93	18.05	1.636	1.239	0.737	0.712	1.544
41	0.5213765	18.101	17.684	17.384	16.945	18.001	1.367	1.017	0.865	0.711	0.934
44	0.5253868	18.156	17.701	17.357	16.942	18.301	1.564	1.326	1.038	0.695	1.152
30	0.5265829	18.182	17.685	17.297	16.933	18.22	1.545	1.295	0.945	0.539	0.768
19	0.5306522	18.152	17.661	17.353	16.943	18.173	1.406	1.253	0.826	0.504	1.063
80	0.53695	18.238	17.735		16.937	18.66	1.152	1.019		0.642	0.378
70	0.5370717	18.048	17.677	17.281	16.808	17.848	0.797	0.879	0.669	0.716	1.084
82	0.5372361	17.993	17.513	17.116	16.732	18.085	1.068	0.834	0.695	0.309	1.423
61	0.5466822	18.257	17.723	17.296	16.905	18.259	0.97	0.727	0.627	0.34	1.038
43	0.5521052	18.411	17.817	17.491	16.971	18.263	1.209	0.878	0.072	0.616	1.212
5	0.5568808	18.175	17.686	17.304	16.911	18.266	1.567	1.227	0.948	0.736	1.184
16	0.5597099	18.187	17.679	17.3	16.889	18.194	1.41	1.111	0.917	0.706	1.239
37	0.564809	18.231	17.709	17.331	16.924	18.163	1.271	1.052	0.781	0.643	1.248
50	0.5657635	18.229	17.745	17.369	16.931	18.241	1.272	1.017	0.754	0.634	1.453
52	0.5714055	18.294	17.768	17.326	16.906	18.159	1.162	0.961	0.786	0.587	0.846
88	0.5725612	17.985	17.526	17.175	16.829	17.943	1.572	1.35	1.11	0.751	1.472
46	0.5747031	18.208	17.703		16.898	18.71	1.434	1.077		0.685	0.29
6	0.5778506	18.144	17.576	17.243	16.743	17.896	1.318	1.063	0.814	0.464	1.007
26	0.5798924	18.295	17.751	17.446	16.919	18.315	1.273	0.949	0.492	0.607	1.009
28	0.5827866	18.217	17.682	17.303	16.878	18.249	1.14	1.013	0.694	0.62	0.681
47	0.5832672	18.068	17.714	17.211	16.86	17.876	1.402	1.071	0.848	0.578	1.004
62	0.5906489	18.269	17.725	17.558	16.914	18.238	1.271	0.989	0.009	0.642	0.695
85	0.5939029	18.338	17.727	17.428	16.893	18.696	0.883	0.808	0.072	0.504	0.021
12	0.5947952	18.272	17.725	17.336	16.916	18.244	1.081	0.854	0.627	0.497	1.032
38	0.5959254	18.244	17.693	17.334	16.902	18.226	1.235	1.069	0.529	0.383	0.725

15	0.5967641	18.097	17.582	17.222	16.81	18.176	1.486	1.289	0.936	0.79	1.125
112	0.5984424	18.322	17.791	17.436	16.928	18.387	0.558	0.384	0.262	0.347	0.826
25	0.6021555	18.24	17.698	17.288	16.881	18.34	1.205	0.955	0.835	0.594	0.981
74	0.6023051	18.138	17.613	17.237	16.815	18.006	1.191	0.954	0.696	0.562	0.921
53	0.6034621	18.312	17.753	17.359	16.936	18.34	0.674	0.532	0.308	0.34	0.486
45	0.6058966	18.301	17.736	17.374	16.893	18.189	0.962	0.772	0.504	0.473	0.392
1	0.6099223	18.212	17.653	17.264	16.834	18.202	1.058	0.913	0.597	0.537	0.481
7	0.6179218	18.253	17.704	17.304	16.857	18.313	1.092	0.823	0.478	0.518	0.567
4	0.6236188	18.239	17.68	17.264	16.836	18.531	1.125	0.847	0.693	0.566	0.23
66	0.6260572	18.312	17.745	17.326	16.892	18.205	0.835	0.698	0.405	0.403	0.674
83	0.6275217	18.211	17.643	17.24	16.83	18.274	1.099	0.954	0.643	0.518	0.552
106	0.6277311	18.336	17.774	17.352	16.9	18.375	0.782	9.299	0.487	0.408	0.491
11	0.6314811	18.242	17.68	17.265	16.843	18.213	0.767	0.626	0.495	0.38	0.728
64	0.6361433	18.217	17.662	17.25	16.83	18.303	0.97	0.783	0.597	0.468	0.607
108	0.6414954	18.315	17.734	17.324	16.888	18.353	0.692	0.522	0.322	0.311	0.504
76	0.6416066	18.433	17.802		16.949	18.271	0.613	0.495		0.355	0.057
20	0.6481624	18.245	17.676	17.258	16.815	18.158	0.962	0.778	0.58	0.454	0.301
36	0.6498354	17.655	17.674	17.26	16.835	18.267	1.014	0.779	0.599	0.506	0.84
22	0.6747379	18.281	17.702	17.437	16.814	18.609	0.821	0.653	0.326	0.422	0.041
72	0.6813507	18.232	17.656	17.225	16.801	18.275	0.69	0.593	0.419	0.381	0.546
167	0.70669	18.106	17.511	17.008	16.629	18.221	0.931	1.027	0.515	0.55	0.723
9	0.7096094	18.127	17.568	17.162	16.73	18.174	0.956	0.772	0.605	0.477	0.773
84	0.7358964	18.166	17.585	17.155	16.703	18.035	0.779	0.603	0.448	0.353	0.477
54	0.7364995	18.123	17.57		16.704	18.412	1.065	0.823		0.525	0.336

RRe						
V	Period (d)	\<I>	\<B-V>	\<V-R>	\<V-I>	\<U-B>
1575	0.279667	17.084	0.374	0.291	0.577	0.146
81	0.2844449	16.637	0.5	0.363	0.737	0.117
153	0.2858137	17.077	0.381	0.254	0.631	0.167
97	0.28825486	17.05	0.381	0.267	0.59	0.131
56	0.28954261	17.08	0.399	0.297	0.624	0.082

RRd						
V	Period (d)	\<I>	\<B-V>	\<V-R>	\<V-I>	\<U-B>
78	0.3457417	17.051	0.498	0.327	0.723	0.200
18	0.3522698	16.993	0.428	0.376	0.746	0.168
65	0.3527580	16.941	0.450	0.341	0.714	0.140
10	0.3532003	16.943	0.475	0.299	0.722	0.026
21	0.3533424	16.963	0.451	0.286	0.745	0.098
51	0.3551330	16.960	0.468	0.341	0.694	0.036
109	0.3555176	17.000	0.470	0.349	0.740	0.191
59	0.3572801	16.968	0.489	0.321	0.700	0.021
87	0.3577057	16.952				0.147
63	0.3577295	16.979	0.475	0.342	0.749	0.090
93	0.3591978	16.940	0.484	0.340	0.731	0.076
73	0.3661399	16.976	0.414		0.705	0.092
42	0.3725726	16.916	0.444	0.360	0.709	0.034
31	0.3617416	16.929	0.468	0.294	0.739	0.184
90	0.3635950	16.895	0.475	0.301	0.705	0.067
8	0.3673849	16.940	0.460	0.415	0.724	0.126
71	0.3693186	16.956	0.478	0.342	0.678	0.152

Table 3.2 Derived parameter values for the RR Lyraes, where V indicates the star number, \<I> is the intensity mean magnitude obtained with the I filter, and B-V, V-R, V-I and U-B indicate the magnitude mean-colors (uncorrected for reddening).

RRc						
V	Period (d)	<I>	<B-V>	<V-R>	<V-I>	<U-B>
103	0.35298342	16.99	0.449	0.344	0.700	0.09
77	0.35464192	16.971	0.442	0.333	0.693	-0.02
92	0.3547447	17.002	0.464	0.328	0.719	0.12
89	0.35538932	16.976	0.457	0.335	0.706	0.112
98	0.35564213	17.016	0.47	0.264	0.703	0.051
111	0.35734358	16.964	0.454	0.286	0.706	0.084
96	0.3584335	16.946	0.467	0.332	0.707	0.073
55	0.3585305	16.961	0.451	0.343	0.703	0.107
434	0.359564	13.648	0.44	0.32	0.719	0.178
32	0.3599885	16.439	0.566	0.416	0.854	0.113
95	0.36264582	16.961	0.468	0.356	0.727	0.073
29	0.36268588	16.956	0.459	0.333	0.69	0.065

RRab						
V	Period (d)	<I>	<B-V>	<V-R>	<V-I>	<U-B>
3	0.4832464	17.002	0.443	0.366	0.715	0.086
40	0.485722	17.116	0.563	0.811	0.791	0.072
34	0.4935571	16.965	0.421	0.193	0.723	-0.206
2	0.4936367	16.949	0.454	0.379	0.726	-0.136
17	0.4980768	16.944	0.483	0.356	0.741	-0.135
49	0.499113	16.98	0.549	0.334	0.718	0.199
14	0.5003413	16.953	0.414	0.364	0.698	0.213
58	0.5005887	16.955	0.498	0.358	0.743	0.055
33	0.5063625	17.162	0.758		0.771	0.029
27	0.5067589	16.952	0.519	0.336	0.745	0.053
23	0.5077039	16.988	0.429	0.375	0.714	-0.187
13	0.5115214	16.925	0.466	0.367	0.725	-0.072
24	0.5165604	16.888	0.499	0.386	0.777	-0.032

57	0.5169378	16.966	0.49	0.375	0.773	0.005
48	0.5197904	16.93	0.477	0.306	0.721	-0.078
41	0.5213765	16.945	0.417	0.3	0.739	-0.1
44	0.5253868	16.942	0.455	0.344	0.759	0.145
30	0.5265829	16.933	0.497	0.388	0.752	0.038
19	0.5306522	16.943	0.491	0.308	0.718	0.021
80	0.53695	16.937	0.503		0.798	0.422
70	0.5370717	16.808	0.371	0.396	0.869	-0.2
82	0.5372361	16.732	0.48	0.397	0.781	0.092
61	0.5466822	16.905	0.534	0.427	0.818	0.002
43	0.5521052	16.971	0.594	0.326	0.846	-0.148
5	0.5568808	16.911	0.489	0.382	0.775	0.091
16	0.5597099	16.889	0.508	0.379	0.79	0.007
37	0.564809	16.924	0.522	0.378	0.785	-0.068
50	0.5657635	16.931	0.484	0.376	0.814	0.012
52	0.5714055	16.906	0.526	0.442	0.862	-0.135
88	0.5725612	16.829	0.459	0.351	0.697	-0.042
46	0.5747031	16.898	0.505		0.805	0.502
6	0.5778506	16.743	0.568	0.333	0.833	-0.248
26	0.5798924	16.919	0.544	0.305	0.832	0.02
28	0.5827866	16.878	0.535	0.379	0.804	0.032
47	0.5832672	16.86	0.354	0.503	0.854	-0.192
62	0.5906489	16.914	0.544	0.167	0.811	-0.031
85	0.5939029	16.893	0.611	0.299	0.834	0.358
12	0.5947952	16.916	0.547	0.389	0.809	-0.028
38	0.5959254	16.902	0.551	0.359	0.791	-0.018
15	0.5967641	16.81	0.515	0.36	0.772	0.079
112	0.5984424	16.928	0.531	0.355	0.863	0.065
25	0.6021555	16.881	0.542	0.41	0.817	0.1
74	0.6023051	16.815	0.525	0.376	0.798	-0.132
53	0.6034621	16.936	0.559	0.394	0.817	0.028

45	0.6058966	16.893	0.565	0.362	0.843	-0.112
1	0.6099223	16.834	0.559	0.389	0.819	-0.01
7	0.6179218	16.857	0.549	0.4	0.847	0.06
4	0.6236188	16.836	0.559	0.416	0.844	0.292
66	0.6260572	16.892	0.567	0.419	0.853	-0.107
83	0.6275217	16.83	0.568	0.403	0.813	0.063
106	0.6277311	16.9	0.562	0.422	0.874	0.039
11	0.6314811	16.843	0.562	0.415	0.837	-0.029
64	0.6361433	16.83	0.555	0.412	0.832	0.086
108	0.6414954	16.888	0.581	0.41	0.846	0.038
76	0.6416066	16.949	0.631		0.853	-0.162
20	0.6481624	16.815	0.569	0.418	0.861	-0.087
36	0.6498354	16.835	-0.019	0.414	0.839	0.612
22	0.6747379	16.814	0.579	0.265	0.888	0.328
72	0.6813507	16.801	0.576	0.431	0.855	0.043
167	0.70669	16.629	0.595	0.503	0.882	0.115
9	0.7096094	16.73	0.559	0.406	0.838	0.047
84	0.7358964	16.703	0.581	0.43	0.882	-0.131
54	0.7364995	16.704	0.553		0.866	0.289

From Table 3.1 we studied the period luminosity relationship of RR Lyraes. We found that the best correlation is with the I absolute magnitude. Figure 3.1 shows a plot with all the RR Lyraes from IC 4499. We found a slope of -0.9, which compared to equation 1.10, shows a poor fit to the model of Catelan *et. al* (2004)
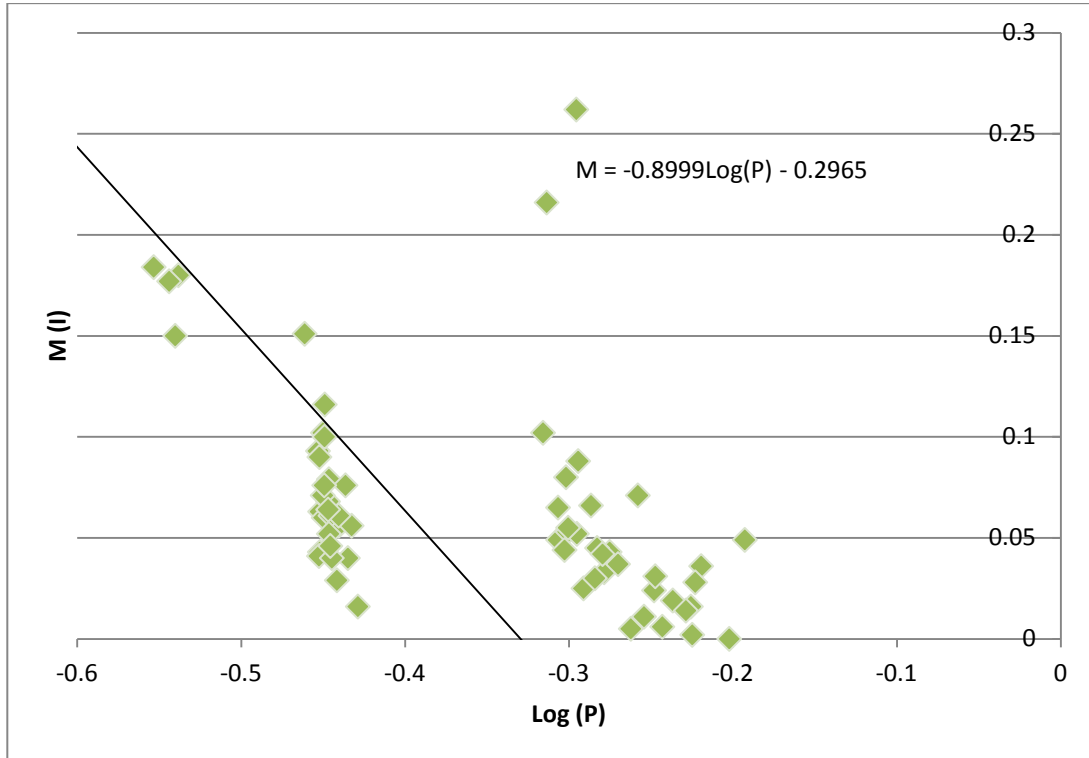
Figure 3.1. Absolute I magnitude vs. logarithmic of the period for all the RR Lyaraes in IC4499. The best fit line indicates a slope of -0.9, compared to theoretical value of -1.1.

However, it is possible to observe subgroups within the total sample of RR Lyraes. Such subgroups correspond to the different categories of RR Lyraes. We found that RRab have a better correlation between period and absolute magnitude (see figure 3.2). We found a slope of -1.4, while equation 1.10 predicts a slope of -1.1. Although these two values indicate a poor

fit, it is possible to observe a more linear correlation when only using RRab stars. Furthermore, the I absolute magnitude was the only magnitude that indicated any correlation with period.
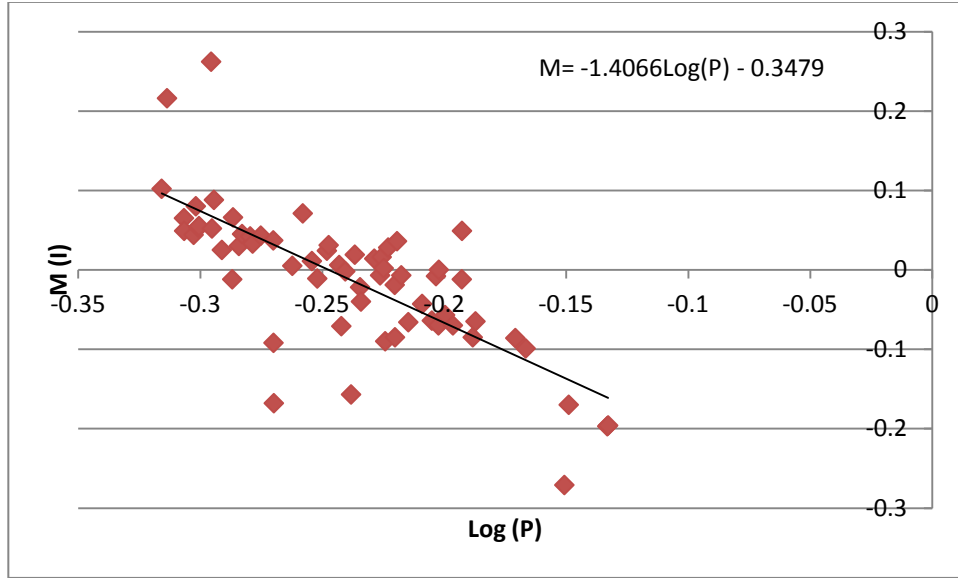
Figure 3.2 Absolute I magnitude vs. logarithmic of period for RRab RR Lyares. A better correlation is seen for this category of RR Lyraes than any other. We found a slope of -1.4 compare to the literature value of -1.1.

C. LIGHT CURVES

We determined five light curves (one for each filter) for each RR Lyrae star. Figure 3.3 shows the light curves of all the RR Lyrae stars in IC 4499. In general the data fitted the templates from the program properly and the light curve shapes were consistent across filters for a given star. However, for most of the stars, the U filter measurements poorly constrained the U filter light curve due to the few data points obtained. The following stars had U light curves that disagreed with the light curves obtained with the other filters: V06, V09, V19, V20, V42, V43, V45, V47, V48, V52, V58, V61, V64, V66, V67, V76, V77, V79, V80, V81, V94, V95, V99

and V112. The shapes of the light curves in all the other filters were consistent within each other (with the exception of V42 and V95). This indicates that the odd shape given by the program to the U filter was caused by too few data points. Similarly the R filter was not shown for V15, V46 and V80 due to insufficient data. Also, V42, V43, V54 and V52 show a poor fit in the R filter. Finally, due to the diverse nature of the data sample, in some cases it was necessary to create multiple light curves in the same filter, depending on when the data were obtained, and then combine them together. In some cases, this method gave us a smooth light curve. However, in other cases we see a shift in the phase of the data. Examples of this are V06 in the V filter, V07 in the V filter, V14 in the V filter, V19 in the V and B filters, V43 in the V filter, V74 in the V and B filters and V12 in the R filter. For V47, V48 and V70 it is possible to observe how the templates from the program differ in shape within the same filter, when the data are split in different sets.

Although there are some inconsistencies between the models and the observed data, overall the light curves obtained for the stars are consistent with the data and allow us to determine the shape of the light curve for each RR Lyrae star. Furthermore, we can conclude that the fit to the templates can only be reliable when sufficient data are available. Previous to this thesis, light curves of RR Lyrae stars for IC 4499 were given by Walker and Nemec (1996). However, they only published the light curves for the V filter. Overall, we can see that the shapes of the curves obtained in this thesis are consistent with those from Walker and Nemec (1996).
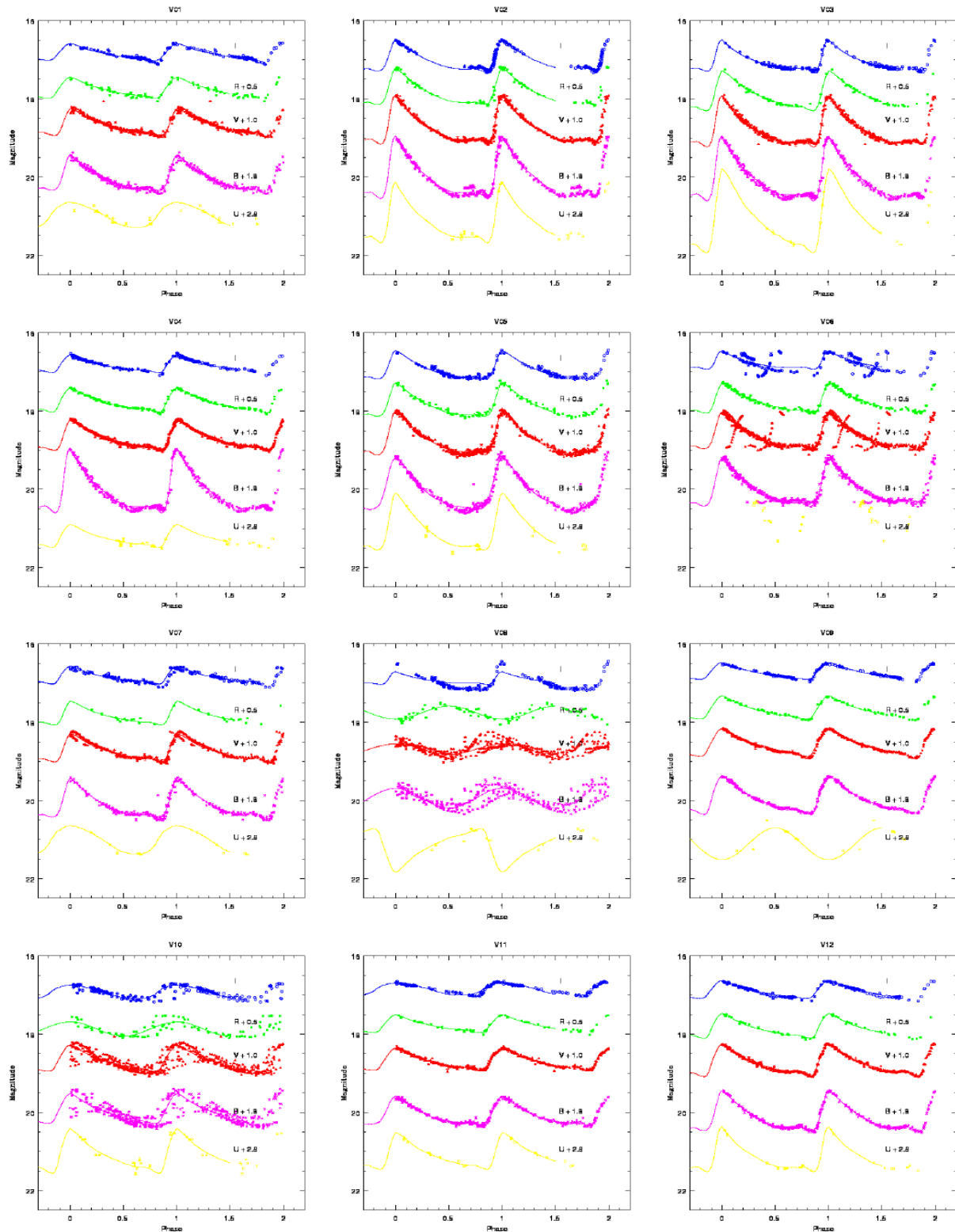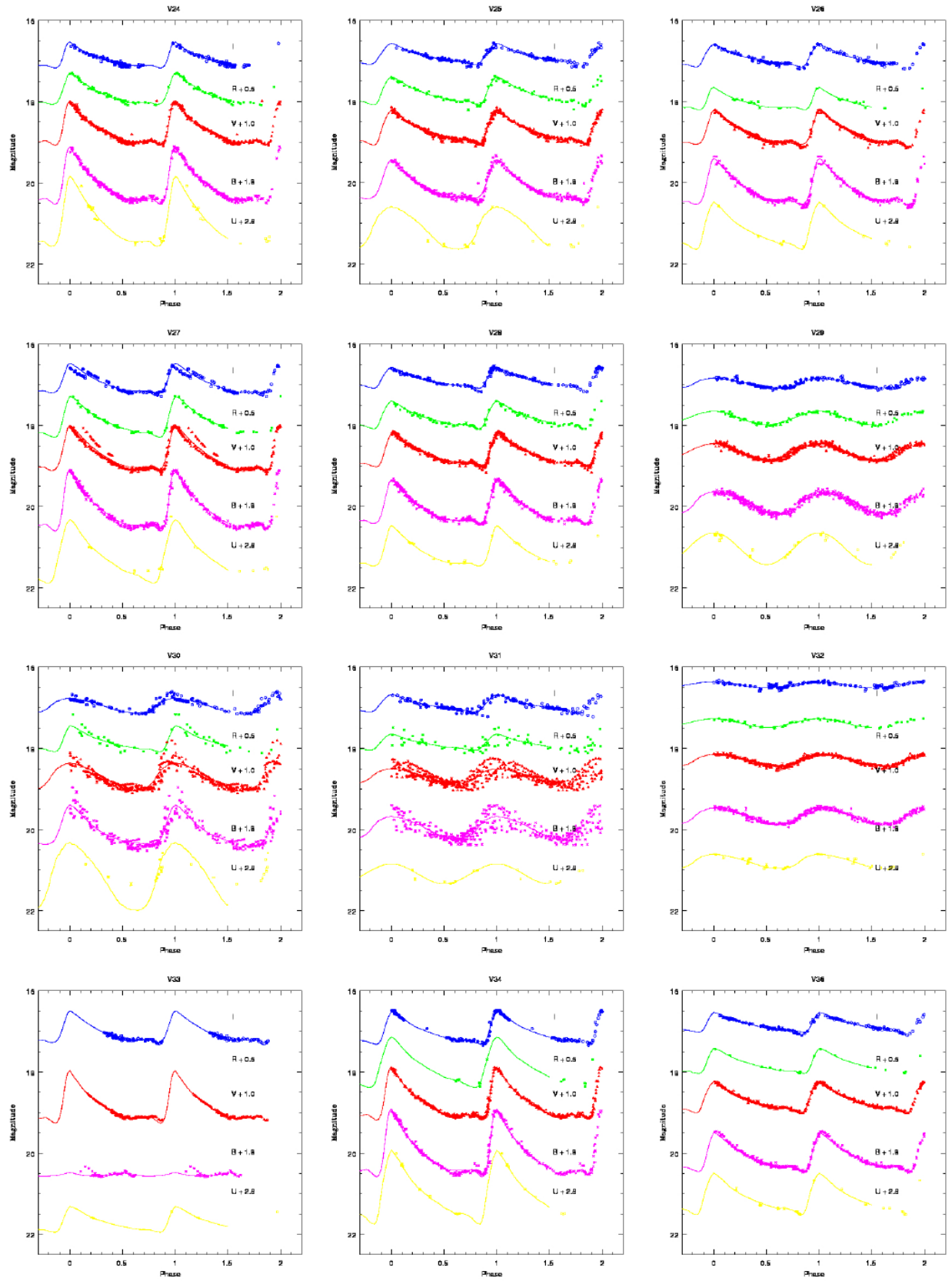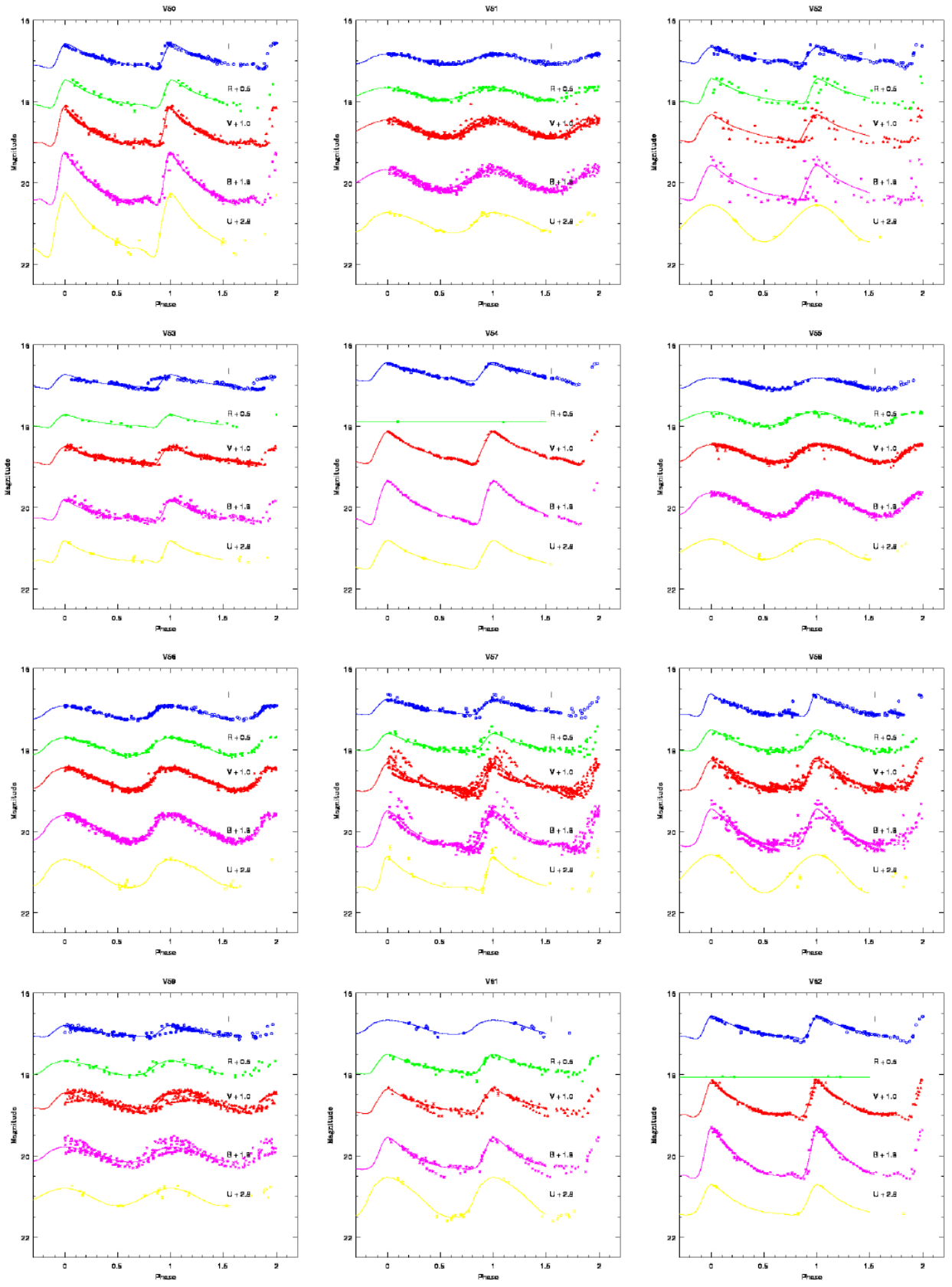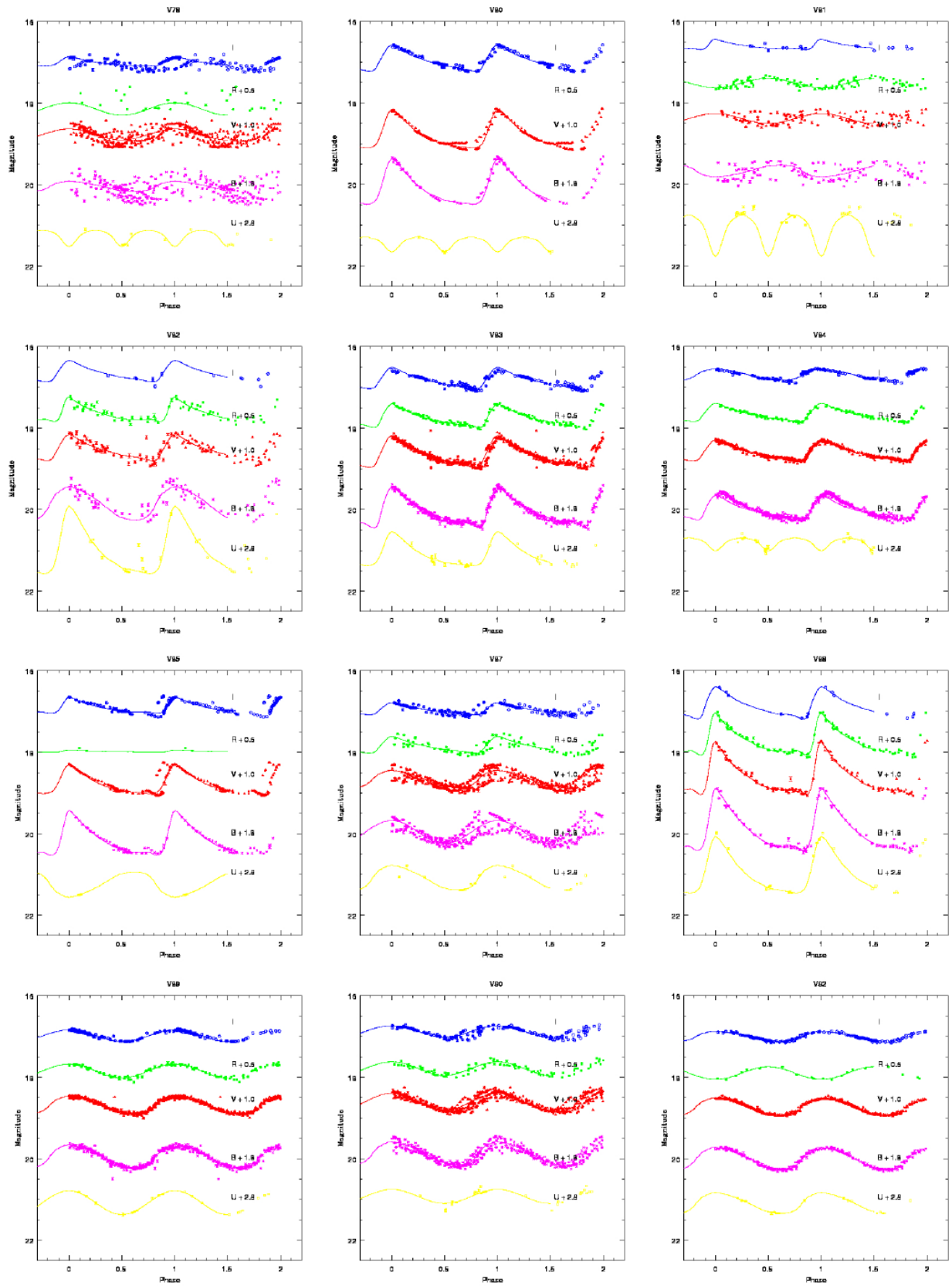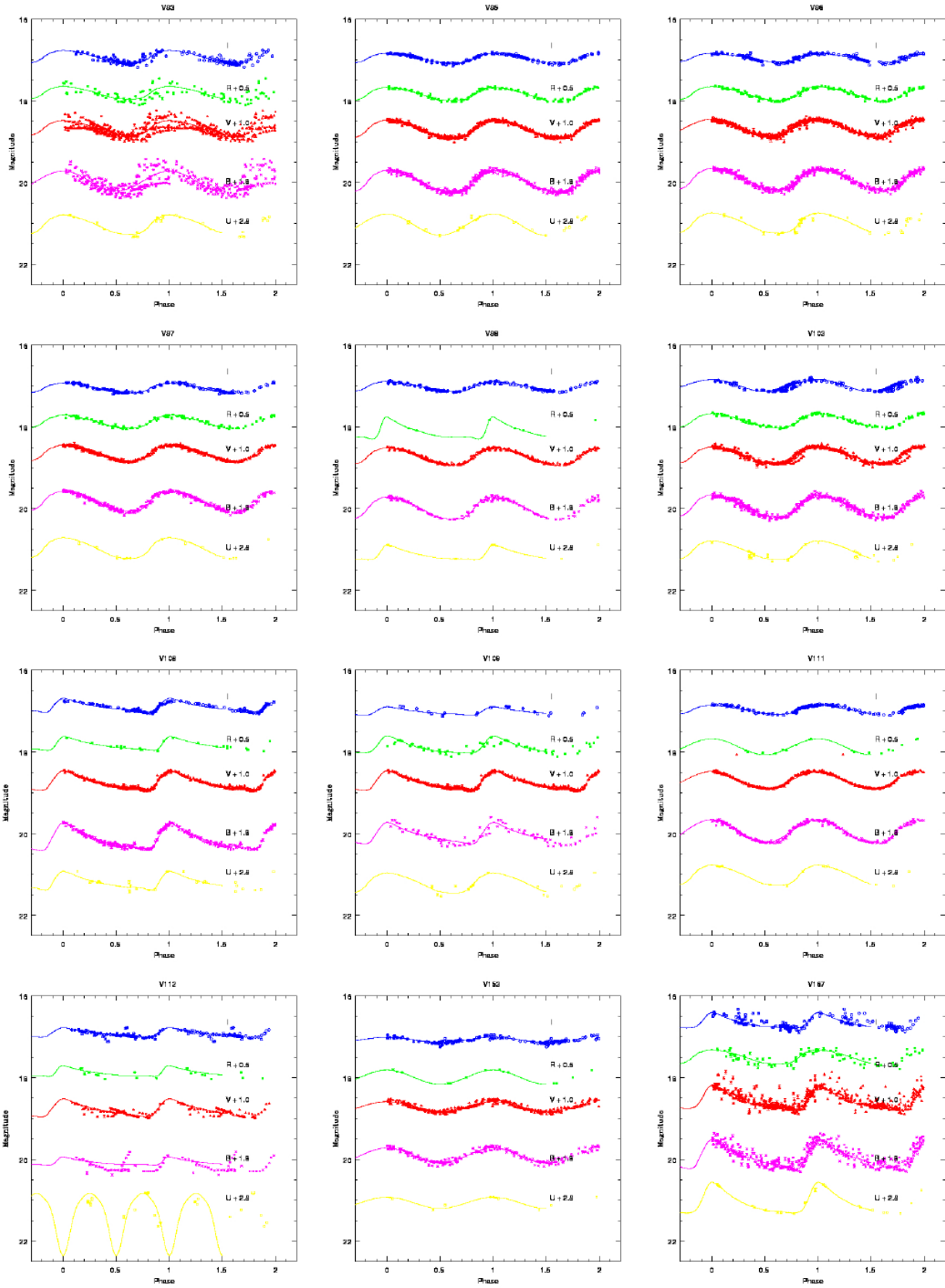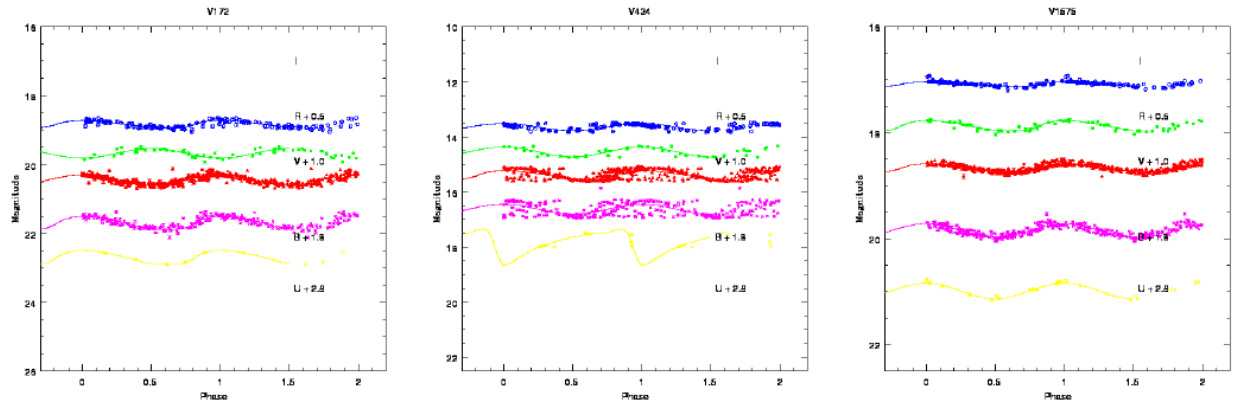
Figure3.3. Light Curves for each of the RR Lyrae stars, in UVBRI filters.

D. THE INSTABILITY STRIP

We found that the stdlc light curve model agreed with our photometric data. Figure 3.4 shows two different plots of V vs. (B-V). The top panel indicates the overlap of the observed magnitudes (black) with those predicted from the theoretical light curves (red). We expect a one to one correspondence between the black points and the red points within the instability strip. However, slight displacements are expected since the red points are obtained from fitting light curves and the black points are from simple averages of the photometry. It can be seen that there is a good overlap between the two sets of data, with similar numbers of red and black points within the IS. However, there are a few black points in the IS that do not correspond to RR Lyrae stars. This indicates a possibility of some non-variable stars within the IS, as mentioned by Walker and Nemec (1996). The close match, within the instability strip, between the distribution of red dots and the black dots in the top panel allows us to use the red dots to determine the color boundaries of the instability strip.

The bottom panel of Figure 3.4 shows the data from the light curve fits (red) overlaid with the data from the synthesis code (green and black). After we had set color boundaries for

the IS, stars predicted by the synthesis code within that range are colored green while non-variable HB stars of both the red and blue groups are shown in black. The boundaries in B-V color were set to include as many red dots as possible, in the lover panel, without including excess stars predicted by the population synthesis model where no RR Lyraes were observed in our sample. We conclude that the instability strip in B-V color is from 0.385 ± 0.005 to 0.62 ± 0.01. A few red dots in the plot lied to the right beyond our assigned red boundary of the IS. These stars had poor photometry and the furthest red dot to the right most probably was not a variable star. The values obtained agree with those of Walker and Nemec (1996) within the uncertainties.
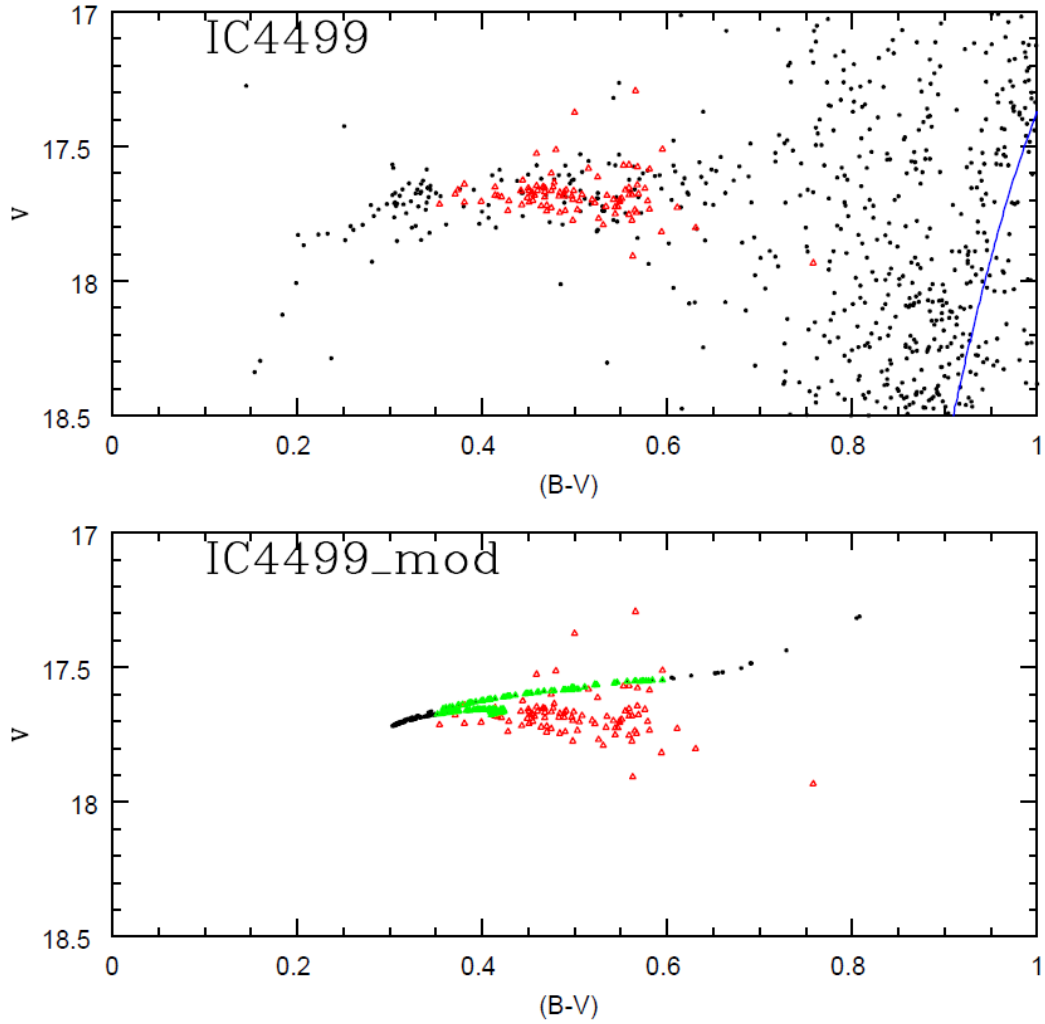
Figure 3.4. Top panel indicates the data observed (black) and the position of the stars estimated by the light curve model (red). Bottom panel indicates the predicted HB stars from the synthesis population model (black), the predicted position of the stars from the light curve model (red), and the stars in the instability strip (green) from the synthesis model.

IV. SUMMARY

We present a study of the RR Lyrae stars in the globular cluster IC4499. Archival data were combined with new data obtained from the 1m telescope at CTIO. The archival data were obtained over a span of 10 years using multiple instruments and telescopes. Photometry and period determination of RR Lyrae stars in the GC were performed by Peter Stetson. I determined the age of the cluster to be $12.5^{+0.5}_{-1.5}$ Gyr by fitting an isochrone curve to the color-magnitude diagram. Furthermore, I obtained light curves, for all the RR Lyraes in IC4499, in 5 different filters, and compared to models in the literature, for which only light curves in the V filter were available. Although for some stars there were not enough data to obtain a light curve in a specific filter, overall we obtained a good agreement for a given star for the shapes of the light curves in different filters. Furthermore, I was able to fill in many of the gaps in the table of measurements by Walker and Nemec (1996) as well as provide new measurements in U band.

I also examined the period-luminosity relationship for RR Lyrae stars, although the correlation found was not tight. It was found that the I filter gives the best fit among those available, agreeing with Catelan *et al.* (2004). Moreover, the RRab stars show a better correlation between the I absolute magnitude and the logarithm of the period.

Finally, we found the instability strip of IC4499 to be the same as that determined by Walker and Nemec (1996), with color limits in B-V = 0.385 and 0.618. The distribution of stars within the different types is unchanged, with the exception of the star V81. This star now agrees with the periods for subtype RRe instead of RRc, although the quality of fit is

unsatisfactory and further confirmation is needed. In general, our results are consistent with those from the previous literature.

Future work will require a better match of a synthesis population code, different than the one we used, with our variable star sample in order to obtain more consistent results. This occurs due to the necessity of scaling the variable star population yielded by the code. Furthermore, more observations of the RR Lyraes are necessary in order to clarify the discrepancy between the periods obtained for V81 by us and by Walker and Nemec (1996). A more precise age for the cluster could potentially be obtained with a finer grid of isochones, as those available were at 1 Gyr intevals.

To determine a better period – luminosity relationship, observations in the K and H filter are necessary, since Catelan *et al.* (2004) indicate that these filters yield the most linear relationship.

REFERENCES

BaStI, http://albione.oa-teramo.inaf.it/

Bradley W. Carrol and Dale A. Ostile, *An introduction to Modern astrophysics* (San francisco:Pearson Addisson Wesley 2007)

Catelan, M., *et al.* 2004, ApJS, 154, 633

Cortes, C. & Catelan, M. 2008, AJ, 177, 362

Dorfi, E. & Feuchtinger, M. 1999, A&A, 348, 815

Ferraro, I. *et al*. 1995, MNRAS, 275, 1057

Gratton, R. *et al*. 2010, A&A, 517, A81

Layden, A. 1998, AJ, 115, 193

Michael Zeilik and Elske v. Smith. Introductory Astronomy & Astrophysics (Philadelphia:Saunders College Publishing 1987

Perryman, M. *et al.* 1195, A&A, 304, 69

Robin, A. *et al*. 2003, A&A, 409, 523

Walker, A. & Nemec, J. 1996, A J. 112,2026

Walker, A. et al. 2011, MNRAS, 415,643

Zinn, R. 1985, ApJS*.*, 293, 424